AIAA 80-0764R

Wing/Store Flutter Suppression Investigation

T. E. Noll,* L. J. Huttsell,* and D. E. Cooley*
Air Force Wright Aeronautical Laboratories, WPAFB, Ohio

The design, testing, and evaluation of active flutter suppression technology using a common wind tunnel model has been successfully completed by the U.S. and several European organizations. This paper emphasizes analytical predictions and presents test data for correlation. Several control laws were evaluated using the FASTOP computer program and a modified Nyquist criterion. Although the design and tests were conducted for a specific Mach number of 0.8, the analyses were performed at several Mach numbers to determine system effectiveness at off-design conditions.

Nomenclature

A/C	= airframe
$\bar{C}$	= wing chord
g	= structural damping coefficient
$\bar{g}$	= acceleration due to gravity
G	= control elements in the forward path of the closed loop block diagram
h	= vertical displacement
H	= control elements in the feedback path of the closed loop block diagram
K	= feedback gain
L	= distance between sensors
M	= Mach number
N	= number of encirclements of the origin made by the Nyquist plot
P	= number of poles of control system open loop transfer function
q	= dynamic pressure
S	= Laplace variable
$\bar{S}$	= wing span
T	= transfer function
V	= velocity
Z	= number of zeros of the characteristic equation with positive real parts
δ	= control surface displacement
Λ	= sweep angle
θ	= torsion slope
ϕ	= bending slope

Abbreviations

B.Ae	= British Aerospace
FASTOP	= Flutter and Strength Optimization Program
FS	= fuselage station
HL	= hinge line
imag	= imaginary
LEC	= leading edge control
MBB	= Messerschmitt-Bolkow-Blohm GmbH
ONERA	= Office National d'Etudes et de Recherches Aerospatiales
TEC	= trailing edge control
WS	= wing station

Subscripts

f	= flutter
F	= filter
IA	= inboard aft
IF	= inboard forward
LE	= leading edge
OA	= outboard aft
OF	= outboard forward
ref	= reference value
TE	= trailing edge

Presented as Paper 80-0764 at the AIAA/ASME/ASCE/AHS 21st Structures, Structural Dynamics and Materials Conference, Seattle, Wash., May 12-14, 1980; submitted June 4, 1980; revision received April 30, 1981. This paper is declared a work of the U.S. Government and therefore is in the public domain.

*Aerospace Engineer, Structures and Dynamics Division, Flight Dynamics Laboratory. Associate Fellow AIAA.

Introduction

STARTING in 1976, the Northrop Corporation supported by the Air Force Wright Aeronautical Laboratories/Flight Dynamics Laboratory (FDL), designed, fabricated, and tested a wing/store flutter suppression system.[1] The flutter model represented an advanced lightweight fighter wing (YF-17) with three different external store configurations. To simulate symmetric flutter characteristics, the semispan flexible wing and fuselage model was designed to be wall mounted with rigid-body pitch and plunge degrees of freedom. Both leading and trailing edge control surfaces (independently actuated by electrohydraulic devices) could be used either singly or in combination for active flutter suppression. The feedback compensation was manually adjustable for various store and flight condition changes. With the cooperation of the NASA Langley Research Center, tests were conducted in the 16-ft Transonic Dynamics Tunnel to define the passive flutter speed of each wing/store configuration, and to obtain improvements in these speeds with active flutter suppression. Only single surface control laws were investigated during these tests. On four separate occasions the model with active flutter suppression was tested to speeds which exceeded the unaugmented flutter condition. A flutter velocity improvement of about 15% was successfully demonstrated.

Beginning in 1978, the model was refurbished and modified for further active flutter suppression wind tunnel investigations. The objective of the follow-on tests was to study new control laws designed by Northrop to provide a 30% improvement in the flutter speed. These control laws were designed for a particular store configuration and tunnel test condition, and used either the leading edge or trailing edge control surface acting alone or together. Through data exchange programs, ONERA (France), MBB (Germany), and B.Ae (United Kingdom) also designed control laws for this model. The Northrop Corporation mechanized these control laws and with the cooperation of NASA, conducted the tests in October 1979. The tested control laws provided significant flutter velocity increases; several increased the flutter speed by 30% or more.

This paper reports on an analytical evaluation by the FDL of control law performance at off-design flight conditions. The international control laws and two of the laws developed and tested by the Northrop Corporation were analyzed and the results are presented herein.

Discussion

This section presents a definition of the analysis methods and modeling procedures used for the stability calculations.

FDL Active Flutter Suppression Model

The FDL active flutter suppression wind tunnel model (Fig. 1) has two active surfaces available for flutter suppression and four accelerometers in the outer wing to measure the model response. The feedback signal can involve any combination of the four sensors or can include a blending of displacements, velocities, and accelerations. A schematic of the model showing planform dimensions, control surfaces, and sensor locations is provided in Fig. 2.

The store configuration selected for the test and for the design of the control laws was an AIM-7S missile mounted on an outboard wing pylon and an empty tip launcher rail (Fig. 1). This configuration was selected because of the clearly defined flutter condition in previous tunnel tests. The violent nature of flutter for this configuration presented a challenging case for evaluating the effectiveness of a store flutter suppression system.

Analysis Procedures

The automated flutter analysis module of the FASTOP Program[2] with the subsonic doublet lattice option[3] was used to perform the unaugmented flutter calculations, and to obtain unsteady aerodynamic forces for the active flutter suppression analysis. For these calculations, two rigid body modes (plunge and pitch), the first seven elastic modes, and a control surface mode were used. All modes used in the analysis had been tuned to match ground vibration test results.

The aerodynamic representation of the flutter model consisted of seven panels that were subdivided into 195 boxes (8 on the forward fuselage, 140 on the wing, 22 on the launcher, 9 on the leading edge surface, and 16 on the trailing edge surface). Both the forward fuselage and the tip launcher rail were represented as flat plates. Aerodynamic interference between the store/pylon and the wing was neglected during these studies. Trend studies were performed by varying the Mach number from 0.6 to 0.95; results at $M=0.8$ are compared with the available test data.

Frequency domain analyses were conducted using the control system interaction program[4] developed for earlier active flutter suppression studies.[5] This program uses a modified Nyquist criterion to determine the augmented aircraft stability characteristics.

The objective of modified Nyquist theory is to determine if any of the complex roots of the characteristic equation, $1+G(S)H(S)=0$, have positive real parts. In this equation, $G(S)$ is the product of all elements in the forward path of the control system, and $H(S)$ is the product of the elements in the feedback loop. Stability can be determined and evaluated using the expression $N=Z-P$, where N is the number of encirclements of the origin made by the plot, Z is the number of zeros of the characteristic equation (factors of the numerator) with positive real parts, and P is the number of poles of the characteristic equation (factors of the denominator) with positive real parts. For a stable system, Z must always be zero which implies that the modified Nyquist plot must encircle the origin P times in a negative (counterclockwise, $N=-P$) direction. If the aircraft speed is below flutter onset, there are generally no poles in the function $G(S)$. The poles of $H(S)$ with positive real parts can be determined from inspection. For the control laws reported herein, there are no poles with positive real parts in $H(S)$. As a result, any clockwise encirclement of the origin would indicate a control system-induced instability. If the aircraft speed is above flutter onset, there will be poles with positive real parts. As a result, there must be one counterclockwise encirclement for each of these poles for the system to be stable.

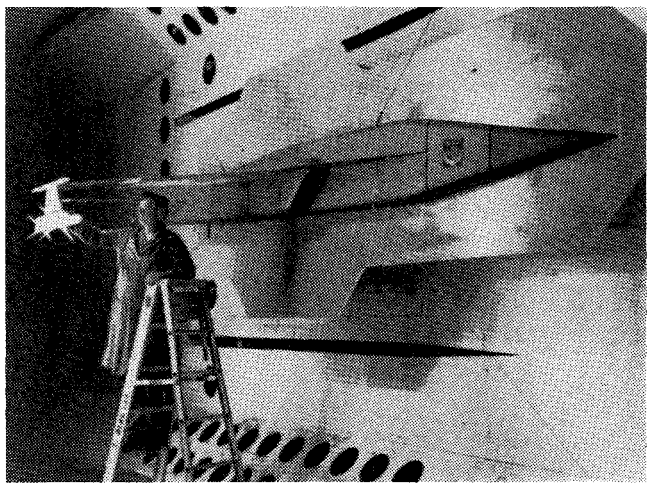

Fig. 1 Active flutter suppression wind tunnel model with AIM-7S missile.

Results

Results of analyses on five different control laws that were tested in the wind tunnel[6] are presented in this section. Analyses were performed at Mach numbers varying from 0.6 to 0.95 to evaluate the off-design characteristics of each control law. The passive and system-on instabilities obtained from the projected test data are also included in the figures for correlation.

Northrop N3 Control Law

A block diagram of the Northrop N3 control law is shown in Fig. 3. By using three sensors, a torsion dominated signal

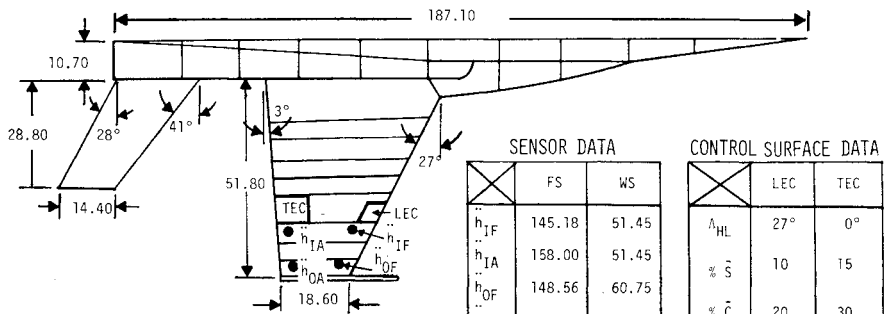

SENSOR DATA

	FS	WS
h_{IF}	145.18	51.45
h_{IA}	158.00	51.45
h_{OF}	148.56	60.75
h_{OA}	157.47	60.75

CONTROL SURFACE DATA

	LEC	TEC
Λ_{HL}	27°	0°
% $\bar{S}$	10	15
% $\bar{C}$	20	30

Fig. 2 Model planform dimensions.

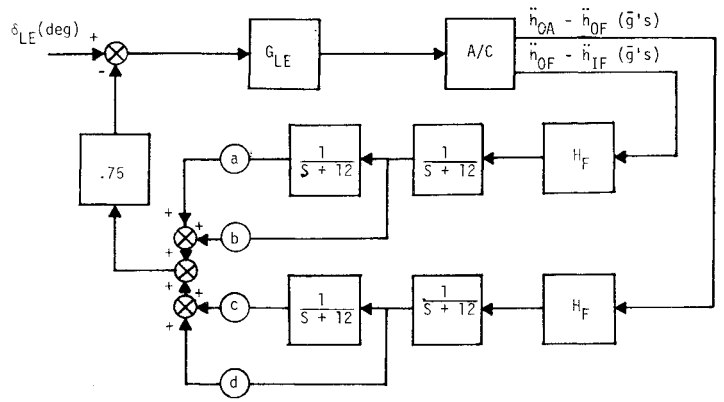

Fig. 3 Block diagram of Northrop N3 control law.

$$H_F = \frac{S^2 + 21.S + 45590.}{S^2 + 299.S + 45590.} \quad \frac{S}{(1 + .03S)(1 + .015S)} \quad \frac{69700.}{S^2 + 264.S + 69700.} \quad \frac{S^2 + 305410.}{S^2 + 552.S + 305410.} \quad \frac{S}{S + 10}$$

$$G_{LE} = \frac{896640.\ (S + 24.)\ (S + 260.)}{(1 + .036S)(1 + .0106S)(S^2 + 204.S + 28900.)(S^2 + 616.S + 193600.)}$$

a = 1158.0 b = -36.5 c = 836.0 d = 35.1

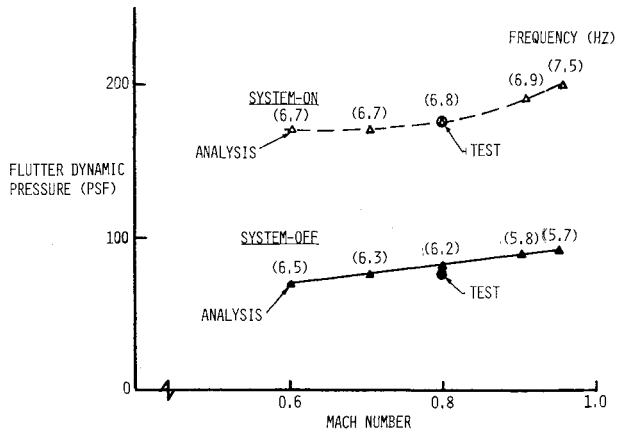

Fig. 4 Mach number effects on flutter, Northrop N3 control law.

($\ddot{h}_{OA} - \ddot{h}_{OF}$) and a bending dominated signal ($\ddot{h}_{OF} - \ddot{h}_{IF}$) are generated and fed back. The feedback loop consists of integrations to obtain component velocities and displacements, and coefficients which blend the four signals to obtain the desirable phase relationship between the bending and torsion modes. A least squares synthesis procedure[7] was used to determine the coefficients. This combined signal drives the leading edge surface. The transfer function H_F contains a series of filters required to avoid ground resonance, and to decouple the flutter suppression system from rigid body and elastic modes. The transfer function G_{LE} represents the leading-edge actuator and was obtained by curve fitting the measured response.

Figure 4 presents the stability boundary in dynamic pressure (pounds per square foot, psf) vs Mach number for the Northrop N3 control law. The unaugmented (system-off) results are also shown. The system-off results show flutter dynamic pressure increasing slightly with Mach number while flutter frequency (shown in parenthesis on the figure) decreases with Mach number. The system-on results show both increasing flutter dynamic pressure and increasing flutter frequencies with Mach number. For the unaugmented model, the flutter dynamic pressure was calculated to be 9% higher than test. With the system-on, the instability was calculated very accurately, only 0.6% higher than the test data. Improvement in dynamic pressure due to the active system was calculated to be 116%, while test data were projected to show 135%. The improvement in the stability boundary due to the active system was calculated to diminish with increasing Mach numbers, varying from 144% at $M = 0.6$ to 112% at $M = 0.95$.

Northrop N1 Control Law

The principal difference between the Northrop N3 and N1 laws is the sensor combinations used. Northrop control law designated N1 provides feedback of vertical acceleration of an outboard sensor ($\ddot{h}_{OF}$) and the wing twist acceleration of the outboard pair of sensors ($\ddot{h}_{OA} - \ddot{h}_{OF}$). The design logic and filters incorporated in this law were identical to the Northrop N3 design. A block diagram of the Northrop N1 law is shown in Fig. 5.

A stability boundary with Mach number for the Northrop N1 control law is presented in Fig. 6. For this control law, a change in the mode of instability was found to cause a very rapid decrease in the dynamic pressure at Mach numbers greater than 0.9. At $M = 0.95$, the analysis indicated that increasing dynamic pressure reduces the gain margin in the pylon side-bending mode (Mode 3) while not noticeably affecting phase margins associated with the wing first-bending mode (Mode 1) or the wing first-torsion mode (Mode 2). For Mach numbers analyzed other than 0.95, loss of control was attributed to decreasing phase margins in the torsion mode. For $M = 0.8$, calculations for control law N1 predicted an instability which is 5% higher in dynamic pressure than the projected experimental point. Calculated improvement in the stability boundary at $M = 0.8$ with the system-on is 152% in dynamic pressure. Test data showed a projected improvement of 163%.

ONERA Control Law

The block diagram for ONERA's control law (Fig. 7) shows the leading edge surface is actuated by a single vertical acceleration ($\ddot{h}_{OA}$). ONERA's design approach is to introduce an effective stiffness change to avoid or delay the coupling of the critical elastic modes. For this application, the torsion mode frequency with system-on does not approach the bending mode frequency as rapidly as when the system is off. The transfer functions defined in the control law consist of a bandpass filter (T_1) and a pseudointegrator (T_2) which was tuned to give low gain at low frequencies to avoid potential rigid body instabilities.

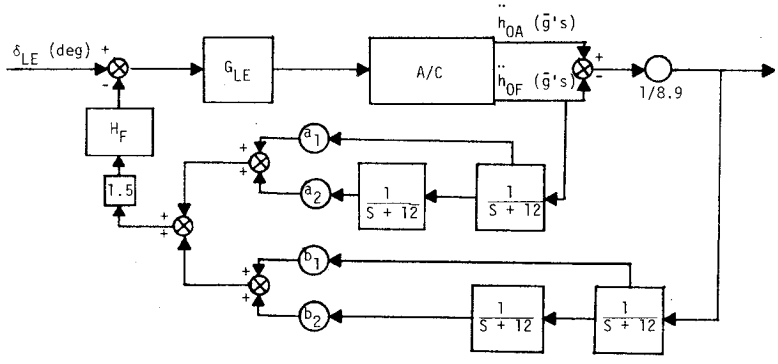

Fig. 5 Block diagram of Northrop N1 control law.

$$G_{LE} = \frac{896640.\ (S + 24.)\ (S + 260.)}{(1. + .036S)\ (1. + .0106S)\ (S^2 + 204.S + 28900.)\ (S^2 + 616.S + 193600.)}$$

$$H_F = \frac{S^2 + 21.S\ \ 45590.}{S^2 + 299.S + 45590.} \quad \frac{S}{(1 + .03S)\ (1 + .015S)} \quad \frac{69700.}{S^2 + 264.S + 69700.} \quad \frac{S^2 + 305410.}{S^2 + 552.S + 305410.} \quad \frac{S}{S + 10}$$

$a_1 = -17.0$ $\quad b_1 = 268.0$

$a_2 = 402.0$ $\quad b_2 = 1284.0$

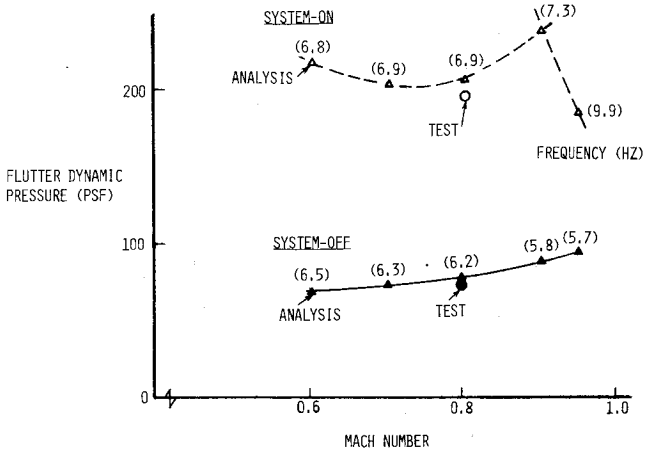

Fig. 6 Mach number effects on flutter, Northrop N1 control law.

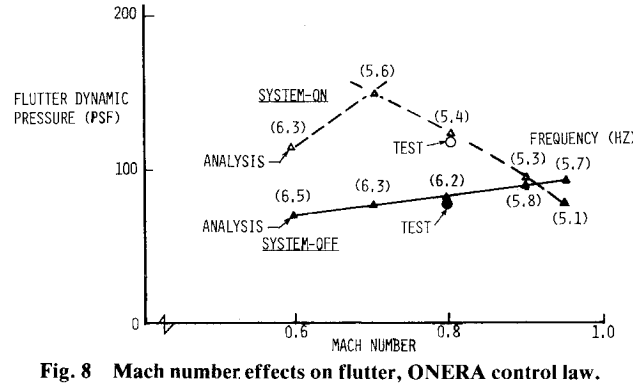

Fig. 8 Mach number effects on flutter, ONERA control law.

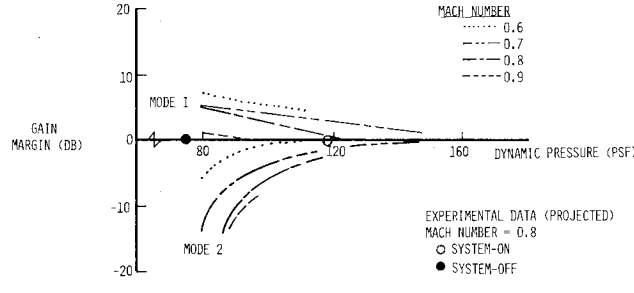

Fig. 9 Calculated gain margins with Mach number, ONERA control law.

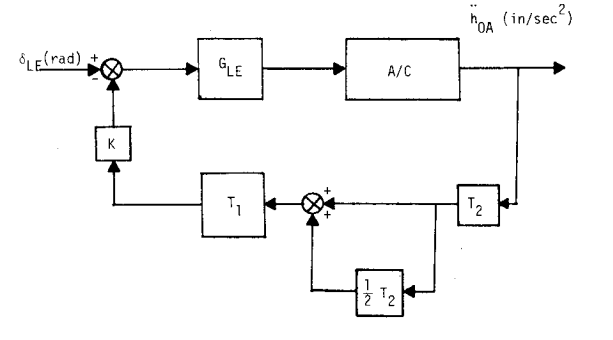

$K = .0009479$

$$T_1 = \frac{.07958S}{(.0001759S^2 + .01015S + 1.)\ (.0001759S^2 + .02451S + 1.)\ (.07958S + 1.)}$$

$$T_2 = \frac{2.5}{.2125^2 + 2.S + 1.}$$

$$G_{LE} = \frac{896640.\ (S + 24.)\ (S + 260.)}{(1 + .036S)\ (1 + .0106S)\ (S^2 + 204.S + 28900.)\ (S^2 + 616.S + 193600.)}$$

Fig. 7 Block diagram of ONERA control law.

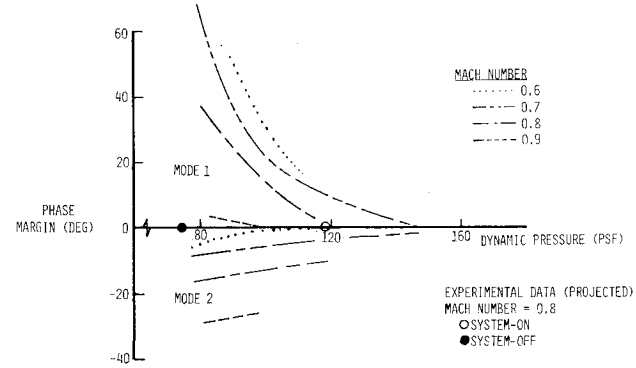

Fig. 10 Calculated phase margins with Mach number, ONERA control law.

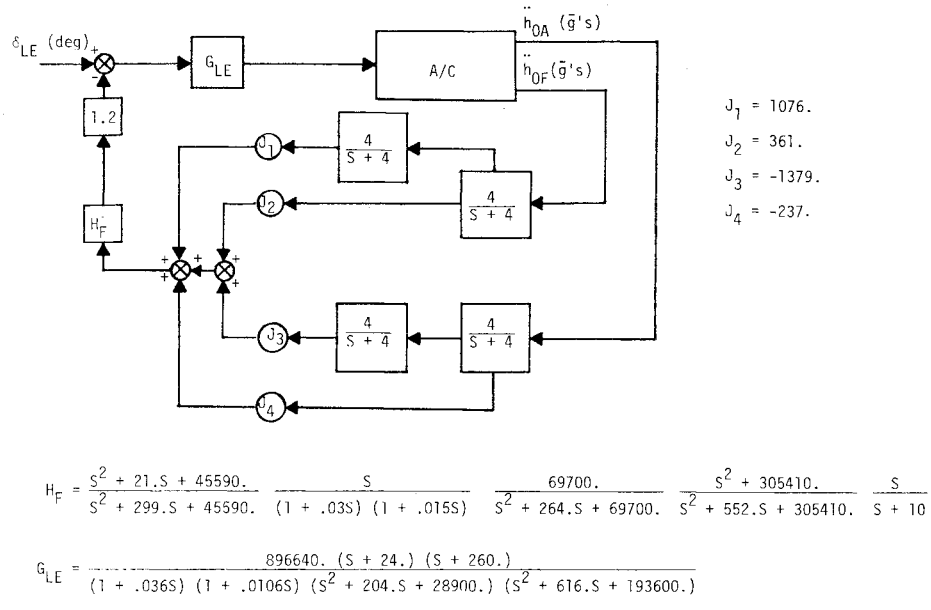

Fig. 11 Block diagram of B.Ae control law.

$$H_F = \frac{S^2 + 21.S + 45590.}{S^2 + 299.S + 45590.} \quad \frac{S}{(1 + .03S)(1 + .015S)} \quad \frac{69700.}{S^2 + 264.S + 69700.} \quad \frac{S^2 + 305410.}{S^2 + 552.S + 305410.} \quad \frac{S}{S + 10}$$

$$G_{LE} = \frac{896640.\ (S + 24.)\ (S + 260.)}{(1 + .036S)\ (1 + .0106S)\ (S^2 + 204.S + 28900.)\ (S^2 + 616.S + 193600.)}$$

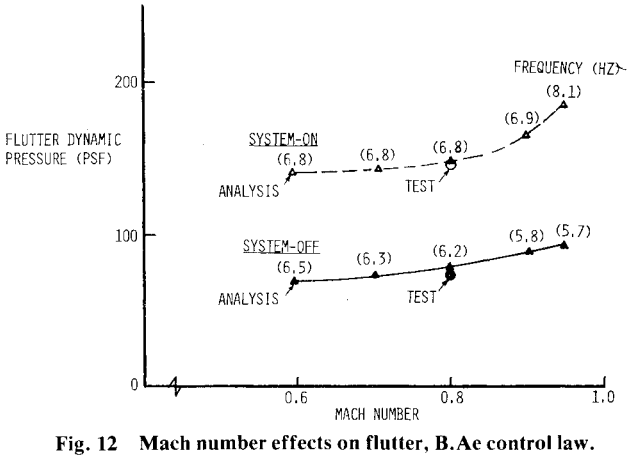

Fig. 12 Mach number effects on flutter, B.Ae control law.

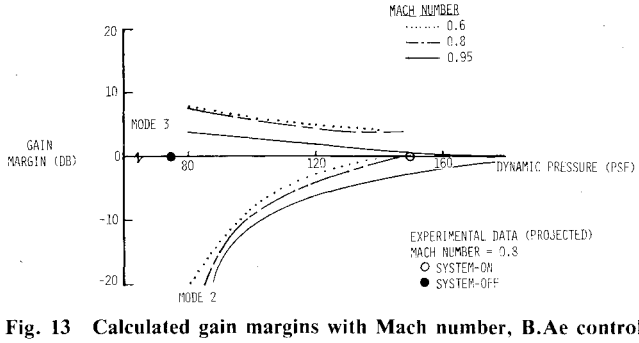

Fig. 13 Calculated gain margins with Mach number, B.Ae control law.

The Mach number trend for this control law is provided in Fig. 8. The control law is most effective at $M=0.7$ where a 95% improvement in flutter dynamic pressure above the passive case is predicted. For Mach numbers less than 0.7, calculations predicted an instability in the torsion mode, while at Mach numbers greater than 0.7, the instability occurs in the bending mode. Also, analysis shows that increasing dynamic pressure at a constant Mach number, causes a phase lead to be introduced into the system. This effect, along with the Mach number effect, results in decreasing instability frequencies with increasing Mach number and a change to the lower frequency bending mode.

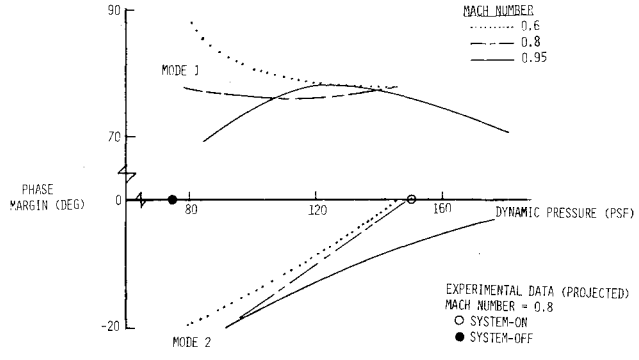

Fig. 14 Calculated phase margins with Mach number, B.Ae control law.

At $M=0.8$, the augmented instability was analytically predicted to occur at 123 psf, which is 3% higher than the projected test result. The analysis shows the performance of the control law to decrease with increasing Mach numbers above 0.7 and predicts a control system induced instability at $M=0.95$. The improvement in the dynamic pressure stability boundary at $M=0.8$ was calculated to be 50%, while test data were projected to show a 59% increase. Figures 9 and 10 show the calculated gain and phase margins, respectively, for the ONERA control law.

B.Ae Control Law

A block diagram of the B.Ae control law is shown in Fig. 11. This law uses two outboard accelerometers ($\ddot{h}_{OA}$ and $\ddot{h}_{OF}$) and four gains acting on the displacement and velocity outputs of the two accelerometers. The four gains were developed using optimal control theory. The design provides a feedback signal to the leading edge servo which approximates a velocity feedback of the flutter mode and gives minimum control surface movement. A series of filters is also included in the control law to avoid adverse interactions with other modes.

The trend of the closed-loop flutter dynamic pressure vs Mach number for the B.Ae control law is shown in Fig. 12. The system-on boundary shows a substantial increase in the flutter speed with increasing Mach numbers. The calculations show an increase in flutter dynamic pressure that varies from 79 to 100% over the Mach number range investigated. In all cases, it is the torsion mode that becomes unstable. At $M=0.8$, the projected test data showed the active system

increased the flutter dynamic pressure by 95%, while the analyses, for the same condition, predicted a 79% increase. The calculated system-on instability in dynamic pressure was about 0.7% above the projected value using test data. The calculations indicate that for the B.Ae control law, increasing Mach number tends to increase the violentness of the instability. The effects of Mach number and dynamic pressure on the gain and phase margins of the B.Ae control law are presented in Figs. 13 and 14.

MBB Control Law

Figure 15 shows the block diagram of the MBB control law. Two inboard sensors are used to obtain torsional accelerations ($\ddot{h}_{IF} - \ddot{h}_{IA}$), and with the use of an inboard and an outboard sensor, accelerations related to bending ($\ddot{h}_{OF} - \ddot{h}_{IF}$) are obtained. These two signals are blended by four optimal coefficients (K_ϕ, $K_{\dot\phi}$, K_θ, and $K_{\dot\theta}$) and compensated by a bandpass filter. For this design, MBB used the doublet lattice unsteady aerodynamic theory for the airloads and ground vibration test results[8] for the modal input data.

For this control law, calculations showed increasing Mach number has a detrimental effect on the stability boundary (Fig. 16). The flutter dynamic pressure is predicted by analysis to decrease from 153 to 112 psf as the Mach number is increased from $M=0.6$ to 0.9. At a Mach number greater than 0.9, the instability is predicted to change to the higher frequency fuselage first-bending mode (Mode 4) causing a further drop in dynamic pressure to 80 psf at $M=0.95$. The analysis predicts the active system to provide 115% improvement in the flutter dynamic pressure at $M=0.6$, and 26% improvement at $M=0.9$. At $M=0.95$, the fuselage bending mode becomes unstable at a dynamic pressure 14% lower than the system-off condition. At $M=0.8$, the system-on flutter dynamic pressure was calculated to be 18% higher than the projected test point. The improvement in flutter

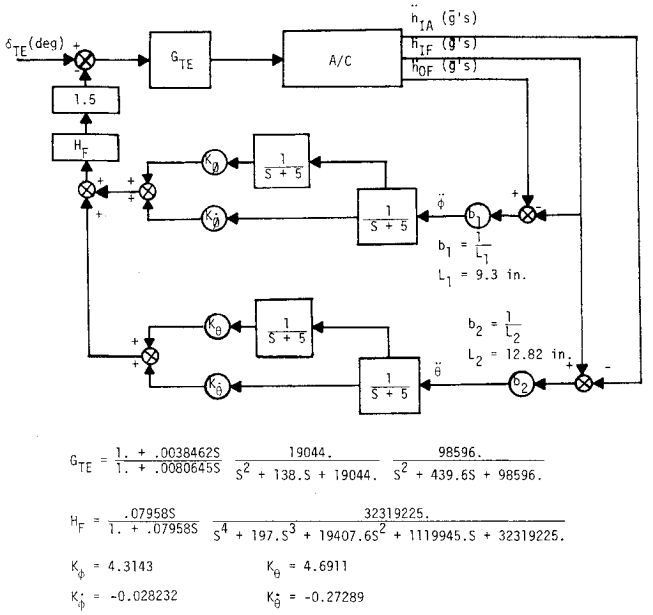

Fig. 15 Block diagram of MBB control law.

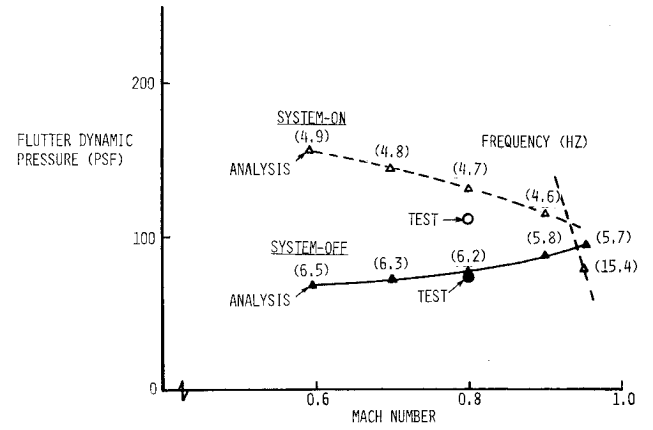

Fig. 16 Mach number effects on flutter, MBB control law.

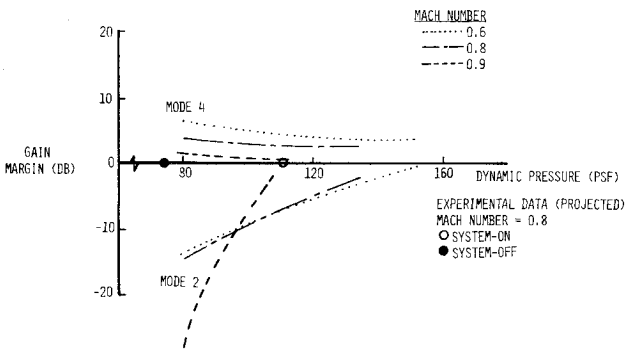

Fig. 17 Calculated gain margins with Mach number, MBB control law.

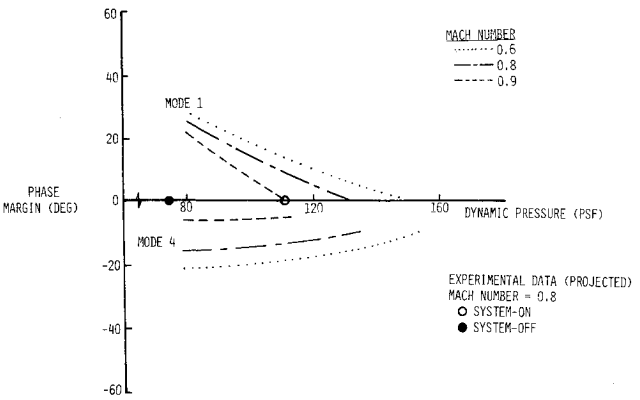

Fig. 18 Calculated phase margins with Mach number, MBB control law.

Table 1 Comparison of calculated and experimental instabilities, $M=0.8$

Control law	Surface	Sensors	q_f, psf Calculated	q_f, psf Experimental
System-off (passive)	...	...	82	75
Northrop N3	LE	$\ddot{h}_{OA}$ $\ddot{h}_{OF}$, $\ddot{h}_{IF}$	177	176
Northrop N1	LE	$\ddot{h}_{OA}$, $\ddot{h}_{OF}$	207	197
ONERA	LE	$\ddot{h}_{OA}$	123	119
B.Ae	LE	$\ddot{h}_{OA}$ $\ddot{h}_{OF}$	147	146
MBB	TE	$\ddot{h}_{OF}$, $\ddot{h}_{IA}$, $\ddot{h}_{IF}$	131	111

dynamic pressure with the active system-on was 48% based on test data, and 60% based on analysis. Figures 17 and 18 present the gain and phase margins, respectively, for the MBB control law.

Analysis Summary

Table 1 presents a summary of the control surfaces and sensors used, the instabilities predicted by analysis and the projected test results at $M = 0.8$ for each control law analyzed. In all cases, the instabilities were predicted by calculations to be higher in dynamic pressure than the test data indicated. This is attributed to the use of calculated control surface aerodynamic loads which would be expected to be higher than experimental values.

Variations in Mach number were shown to have a significant effect on control law performance. Changing the Mach number from the design condition was shown to be either beneficial or detrimental, depending on the control law. For several cases, variations in Mach number resulted in a change of the principal structural mode involved in the instability. In some cases, control system-induced instabilities in both low and high frequency modes were predicted at off-design Mach numbers. For this model, increasing Mach number added phase lead to the system, while increasing dynamic pressure provided either phase lead or phase lag depending on the control law. For those cases where a change in the mode of instability occurs, it is attributed to a combination of these two effects (lag resulted in higher frequency mode instabilities while lead resulted in lower frequency instabilities). For an operational system, the gain and phase would have to be adjusted based on flight conditions to improve the stability margins.

References

[1] Hwang, C., Winther, B.A., and Mills, G.R., "Demonstration of Active Wing/Store Flutter Suppression Systems," AFFDL-TR-78-65, June 1978.

[2] Wilkinson, K. et al., "An Automated Procedure for Flutter and Strength Analysis and Optimization of Aerospace Vehicles," AFFDL-TR-75-137, Vols. I and II, Dec. 1975.

[3] Giesing, J. P., Kalman, T.P., and Rodden, W. P., "Subsonic Unsteady Aerodynamics for General Configurations," AFFDL-TR-71-5, Part I, Vols. I and II, Nov. 1971.

[4] Noll, T.E. and Huttsell, L.J., "Control System/Airframe Interaction Analyses for the YF-16 Missile-On Configuration," AFFDL-TM-77-3-FBR, March 1977.

[5] Triplett, W.E., Kappus, H.-P. F., and Landy, R.J., "Active Flutter Suppression Systems for Military Aircraft, A Feasibility Study," AFFDL-TR-72-116, Feb. 1973.

[6] Hwang, C., Johnson, E.H., Mills, G. R., Noll, T.E., and Farmer, M.G., "Wind Tunnel Tests of the Improved Wing/Store Flutter Suppression System, An International Effort," AGARD Report 689, April 1980.

[7] Johnson, E.H., "Active Flutter Suppression Control Law Definition Via Least Squares Synthesis," AIAA Paper 80-0765, May 1980.

[8] Voelker, L.S., "Ground Vibration Tests of the Active Flutter Suppression Transonic Model with External Stores," AFFDL-TM-77-92-FBR, Dec. 1977.